Journal of Power Sources 211 (2012) 52–58

Contents lists available at SciVerse ScienceDirect

Journal of Power Sources

journal homepage: www.elsevier.com/locate/jpowsour

High-performance $LiFePO_4$/C materials: Effect of carbon source on microstructure and performance

Quan-Bing Liu, Shi-Jun Liao, Hui-Yu Song, Zhen-Xing Liang*

Key Laboratory for Fuel Cell Technology of Guangdong Province, School of Chemistry and Chemical Engineering, South China University of Technology, 381, Wushan St., Guangzhou 510641, China

ARTICLE INFO

Article history:
Received 6 December 2011
Received in revised form
31 January 2012
Accepted 29 March 2012
Available online 13 April 2012

Keywords:
Hybrid carbon sources
Lithium ion battery
Lithium iron phosphate
Spray drying-carbothermal method

ABSTRACT

In this work, high-performance $LiFePO_4$/C materials are successfully prepared by a spray drying-carbothermal method. The effect of the carbon source (*viz.* inorganic, organic and their hybrid) is extensively investigated on the microstructure and electrochemical property of the composite materials. Vulcan XC-72, an inorganic carbon additive, can remarkably improve the electronic conductivity of the composite material; however, the resultant large crystallite size and low specific surface area limit the Li ion diffusion and thereby lower the electrochemical performance. As a typical organic carbon additive, glucose yields mesoporous $LiFePO_4$/C particles with a much higher specific surface area and smaller crystallite size; however, the electronic conductivity of the pyrolyzed carbon is insufficiently high for the real applications. By using the dual hybrid carbon sources, the synthesized $LiFePO_4$/C material features a high electronic conductivity, large specific surface area, small grain size, and the formation of mesopores. In line with these advantages, the composite yields the best electrochemical performance with the discharge capacity of 168.1 mAh g^{-1} at 0.1 C, which is approximate to the theoretical capacity. This material also performs well at high rates with discharge capacities of 122.0 and 93.0 mAh g^{-1} at 5.0 and 10.0 C, respectively.

1. Introduction

The olivine $LiFePO_4$ (LFP) is a promising cathode material in lithium ion batteries (LIBs) due to the advantages including high capacity, structural stability, flat charge/discharge plateaus, environmental benignity, excellent safety, low-cost [1–4]. However, the charge/discharge capacity is generally much lower than the theoretical value, especially at high current rates, which seriously retards its real application. The reason can be attributed to the poor electronic conductivity ($\sigma_e \sim 10^{-9}$ S cm^{-1}) [5] and low ion diffusion coefficient ($D_{Li}^{+} < 10^{-14}$ cm^2 s^{-1}) [6]. Therefore, high electronic conductivity, low ionic diffusion resistance, effective interfacial electrode/electrolyte contact are highly desirable for the electrode materials to achieve the high rate capabilities in LIB.

Tremendous work has been devoted to synthesize the above-featured materials [7–10], which includes: i) Surface coating with carbon has been proved effective to improve the electronic conductivity. ii) Decreasing the particle size can significantly shorten the diffusion distance and thus lower the ionic diffusion resistance. iii) Constructing the mesopores in the composite materials can remarkably increase the specific surface area, which favors the interfacial contact of electrode/electrolyte. For example, Wu et al. [11] dispersed the $LiFePO_4$/C nanoparticles in a nanoporous carbon matrix by a sol–gel method, which yields a superior cathode performance in LIB. They suggested that both the small particle size of $LiFePO_4$ and the use of a nanoporous carbon matrix could effectively enable Li^+ and e^- to migrate and reach the active particle, hence realizing the full potential of the nanoactive materials. Similarly, Zhao et al. [12] deposited the $LiFePO_4$ particles on the tridimensional porous carbon framework, which showed high specific surface area and thereby superior electrochemical performance. Saravanan et al. [13] prepared the nanoplate $LiFePO_4$ material by a solvothermal method, which was coated with a 5 nm thick amorphous carbon layer. The thin layer of the nanoplate favored a short diffusion length for Li^+ ions, and the carbon coating facilitated the electron diffusion, thereby resulting in a high rate performance. Wang et al. [14] reported an in-situ polymerization restriction method to prepare the nanometer-sized $LiFePO_4$/C composite with a core–shell structure, which also yielded an excellent electrochemical performance.

Among the various efforts, the carbon coating during the synthesis yields coupled effects on the morphology and microstructure of the

* Corresponding author. Tel./fax: +86 20 87113586.
E-mail addresses: zxliang@hotmail.com, zliang@scut.edu.cn (Z.-X. Liang).

0378-7753/$ – see front matter © 2012 Elsevier B.V. All rights reserved.
doi:10.1016/j.jpowsour.2012.03.090

resultant materials, thereby determining the ion/electron diffusion, the interfacial contact and electrochemical performance of $LiFePO_4$/C. A variety of the carbon sources have been employed in the synthesis, such as citric acid [15], sucrose [16], tartaric acid [17] and carbon black [18]. However, it seems to be somewhat arbitrary to select the carbon source in the previous work.

In this work, we extensively investigate the effect of the carbon source on the microstructure and the performance of the $LiFePO_4$ material. And for the first time, we report that by using the dual organic/inorganic carbon sources, the synthesized $LiFePO_4$/C composite material features a small crystal grain size, mesoporous structure, high specific surface area and decent electronic conductivity. As a result, the composite material yields a superior electrochemical performance and rate capability in LIBs.

2. Experimental

2.1. Synthesis of $LiFePO_4$/C composites

The $LiFePO_4$/C composite was prepared by a two-step method. First, the precursors were dissolved in an aqueous solution, which was then spray-dried to form precursor powders. Second, the solid precursor powders experienced carbothermal reduction in an inert gas at high temperatures, producing the $LiFePO_4$/C composite. More details are described as follows.

First, 0.300 mol $(FeNO_3)_3 \cdot 9H_2O$ (AR), 0.300 mol $(NH_4)_2HPO_4$ (AR) and 75.0 g glucose were dissolved in 120 mL deionized (DI) water. Then, under vigorously stirring, the above solution was poured into a Li-precursor aqueous solution containing 0.300 mol LiOH (AR) in 70 mL DI water, yielding a gel-like mixture. The gel mixture finally turned to be a sol upon adding 10.0 mL strong aqua ammonia. The precursor sol was spray-dried in a centrifugal disc spray dryer at a rate of 30 mL min^{-1} with inlet and outlet temperatures at 220–260 °C and 110–120 °C, respectively. Finally, the resultant precursor powders were pyrolyzed at 750 °C for 10 h in a tube furnace under nitrogen atmosphere. The resultant $LiFePO_4$/C composite material was referred to as LFP-OC, as the organic carbon glucose was used as the sole carbon source in the synthesis.

The $LiFePO_4$/C composite material prepared with the inorganic carbon source, LFP-IC, was synthesized in the same route except that glucose was substituted by 14.0 g Vulcan XC-72 carbon powders. Similarly, the $LiFePO_4$/C composite material prepared with dual carbon sources, LFP-DC, was synthesized by adding 50.0 g glucose and 5.00 g Vulcan XC-72 carbon powders.

We further prepared another two LFC-DC samples with different amounts of the dual carbon sources, viz. LFP-DC-I with 60.0 g glucose and 2.00 g Vulcan XC-72 carbon, LFP-DC-II with 35.0 g glucose and 8.00 g Vulcan XC-72.

In this work, the content of the residual carbon was kept identical for all the synthesized $LiFePO_4$/C composites.

2.2. Physical characterization

X-ray diffraction (XRD) pattern was obtained with a Rigaku D/max-2200 X-ray diffractometer. Scanning electron micrograph (SEM) and elemental mapping were taken on a Hitachi S-4800 equipped with energy dispersive spectroscopy (EDS). The N_2 adsorption–desorption isotherms were measured with Tristar ASAP 2010 gas adsorption analyzer. The specific surface area was calculated by the Brunauer–Emmett–Teller (BET) analysis, and the pore size distribution was calculated by the Barret–Joyner–Halenda (BJH) method. The carbon content was determined with a carbon–sulfur analyzer (Leco, CS-444LS, USA).

The electronic conductivity of the $LiFePO_4$/C pellet was measured by the four-point probe method using a contact-type conductivity meter (Suzhou Tong-Chang. SZT-2A, China). The composite pellet was fabricated as follows. $LiFePO_4$/C powder was mixed with 5 wt.% polyvinylidene fluoride (PVDF), which was then pressed under 20 MPa for 5 min to form the pellet.

2.3. Electrochemical test

The electrochemical evaluation of the $LiFePO_4$/C composite material was performed with a CR2016-type coin cell. The composite powder, acetylene black and PVDF binder were mixed at a weight ratio of 90:5:5 in N-methyl-2 pyrrolidinon (NMP). The cathode loading onto aluminum foil was about 7–10 mg cm^{-2} 1.0 M $LiPF_6$ in a liquid mixture containing 1:1 by volume ethylene carbonate: dimethyl carbonate (EC:DMC) were used as the electrolyte.

The coin cell was evaluated by the galvanostatic charge and discharge between 2.0 and 4.2 V (vs. Li^+/Li) on a battery evaluation system (New ware, CT-3008, China). The cells were charged to 4.2 V at 0.1 C, and discharged to 2.0 V at different current rates. The discharging capacity was then calculated by deducting residual carbon; in other words, the capacities reported herein are merely based on the active material ($LiFePO_4$).

3. Results and discussion

3.1. Structure characterization

Fig. 1 shows the XRD patterns of the three $LiFePO_4$/C materials prepared with the inorganic carbon source (LFP-IC), organic carbon source (LFP-OC) and the dual carbon sources (LFP-DC). The peaks of the three samples agreed well with the orthorhombic phase $LiFePO_4$ in the standard Powder Diffraction Card (PDF Card No. 40-1499), and no impurities were detected, which indicates that the high-purity $LiFePO_4$/C composite could be synthesized by this method. The average diameter of the $LiFePO_4$ crystallite can be estimated by using Debye–Scherrer equation, and the results were listed in Table 1. It is seen that the diameter increases in the order of LFP-OC (30.3 nm) < LFP-DC (31.6 nm) < LFP-IC (47.2 nm), indicating the presence of the organic carbon source can effectively lower the crystallite size. Such an effect can be understood as follows. The organic carbon glucose can be uniformly mixed with other precursors at the molecular level in the precursor sol. During the spray drying process, glucose may be uniformly dispersed in the aggregates or reside on the surface, which then acts as the stabilizer

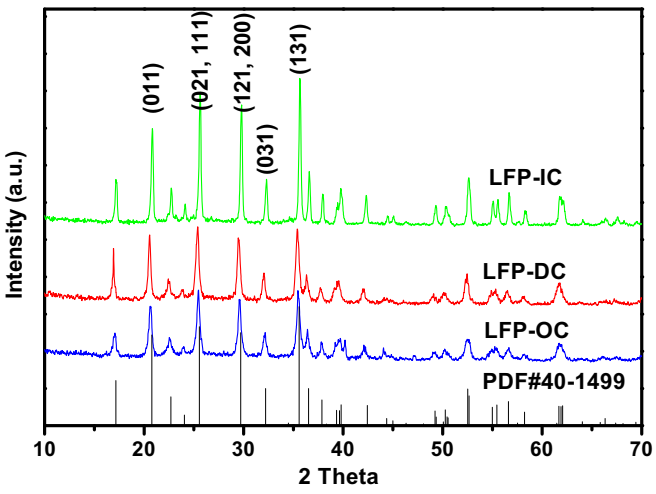

Fig. 1. XRD patterns of the three $LiFePO_4$/C materials prepared with the inorganic carbon source (LFP-IC), organic carbon source (LFP-OC) and the dual carbon sources (LFP-DC).

Table 1
Grain size, specific surface area, electronic conductivity and carbon content for the $LiFePO_4$ composites prepared with different carbon sources.

Sample	Grain size (nm)	Specific surface area ($m^2\ g^{-1}$)	Conductivity ($S\ cm^{-1}$)	Residual carbon (wt. %)
LFP-OC	30.3	125.8	7.9×10^{-4}	14.3
LFP-DC	31.6	114.9	2.4×10^{-2}	14.2
LFP-IC	47.2	17.2	6.4×10^{-2}	13.8

and therefore prevents the nanocrystallites against the coalescence. In comparison, the inorganic carbon with the particle diameter of 30–40 nm cannot be uniformly mixed with the precursors, finally yielding the larger crystallites.

3.2. Morphology characterization

Fig. 2 shows the SEM images of the $LiFePO_4$/C composites prepared with different carbon sources. Fig. 2a–c displays the panoramic morphologies of the $LiFePO_4$/C composites prepared with glucose, glucose/carbon XC-72R, carbon XC-72R, respectively. It is seen that the synthesis method can yield $LiFePO_4$/C microspheres with a fairly uniform size distribution of 5–10 μm. Detailed investigation on the microstructure is shown in Fig. 2d–f. It can be seen that each microsphere are actually comprised of smaller primary particles. Fig. 2d,e suggests that the primary particles are rather uniform in diameter of ca. 50 nm for the $LiFePO_4$/C composites synthesized with glucose as the carbon source. In comparison, the particle size is not uniform and much larger when merely inorganic carbon was used, as seen in Fig. 2f. Element mapping (See Fig. S1) results suggest that the irregular block particles should be $LiFePO_4$ but not carbon, indicating that carbon and $LiFePO_4$ cannot be mixed at a molecular level. Based on the SEM results, we can conclude that the organic carbon source is essential to synthesize the composite material with uniform primary particles and carbon doping, which agrees well with the previous findings.

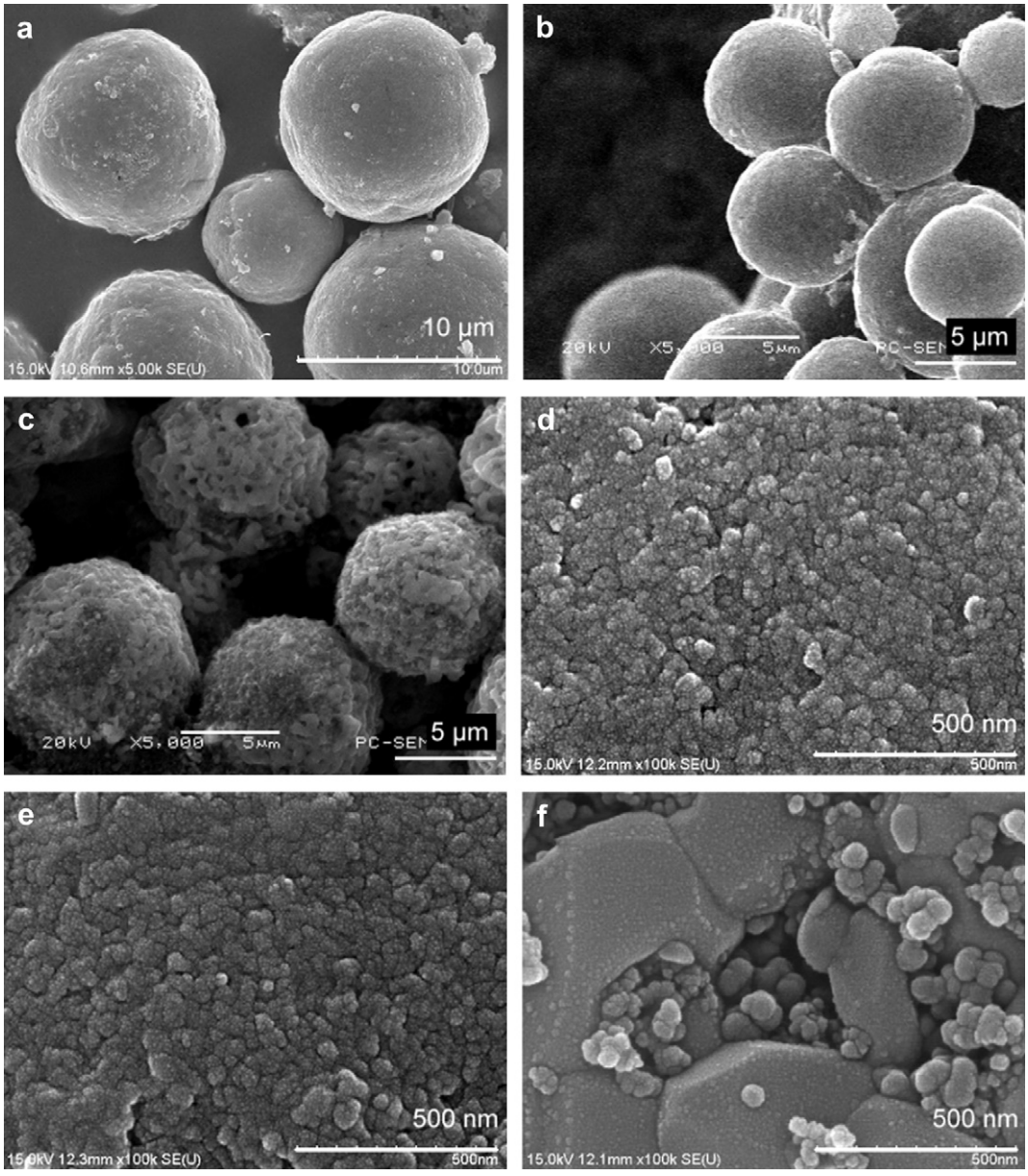

Fig. 2. SEM images of the $LiFePO_4$/C composites: (a, d) LFP-OC; (b, e) LFP-DC; (c, f) LFP-IC.

3.3. Pore structure and specific surface area

The pore structure of the synthesized $LiFePO_4$/C composite was characterized by the nitrogen ad/desorption isotherms. Fig. 3 shows the isotherm curves of the three composite samples, viz. LFP-OC (Fig. 3a), LFP-DC (Fig. 3b) and LFP-IC (Fig. 3c). It is seen that the two former isotherm curves are basically similar in shape, which considerably differs from Fig. 3c. Fig. 3a,b indicate that LFP-OC and LFP-DC display type IV isotherms with H3 hysteresis loops, which suggest the two composites are typical mesoporous materials. In comparison, as seen in Fig. 3c, the isotherm of LFP-IC can be ascribed to Type II and is rather similar to the pure carbon XC-72R, indicating a nonporous structure when the carbon XC-72R was used as the sole carbon source. The pore structure of the three composites can further be confirmed by analyzing the pore size distribution, as seen in the inset of Fig. 3. LFP-OC and LFP-DC show a pore size distribution in the range of 5–30 nm, confirming that the two composites are of typical mesoporous structures. The formation of the mesopores can be ascribed to the glucose decomposition during the pyrolysis of the precursor. Based on the above findings, it can be concluded that the organic carbon precursor is essential to yield the mesoporous structure of $LiFePO_4$/C. The mesoporous structure of both LFP-OC and LFP-DC will favor the entrance of electrolyte into the electrode, which facilitates the interfacial contact between the electrolyte and the $LiFePO_4$/C composite [19].

We also calculated the total specific surface area by the BET analysis, as seen in Table 1. The LFP-OC and LFP-DC composites synthesized with glucose possess one order of magnitude larger specific surface areas than does LFP-IC. For the composite with the organic carbon source, the higher specific surface area can be attributed to the smaller grain size and mesoporous nature of the two composites, as discussed above. It is understandable that a high specific surface area will also facilitate its interfacial contact with the electrolyte [20–22], thus shortening the diffusion distance of Li^+ and lowering the concentration polarization in the electrode [23].

3.4. Electronic conductivity

Electronic conductivity of the cathode material is another key issue to determine the electrochemical performance of the battery. Table 1 lists the electronic conductivity of the three composites. It is seen that the LFP-IC and LFP-DC composites yield two order of magnitude higher electronic conductivities than does LFP-OC while keeping the residual carbon content the same. It is thus concluded that the addition of the inorganic carbon source is essential to achieve a high electronic conductivity. The reason is that the inorganic carbon XC-72R has more graphitic carbon than does the graphitized carbon decomposed from glucose [24–26].

In summary, we believe that the $LiFePO_4$ composite synthesized with the dual carbon sources features a mesoporous nature, small grain size, high specific surface area, and superior electronic conductivity, which will thereby contribute to a superior electrochemical performance in the Li-ion battery.

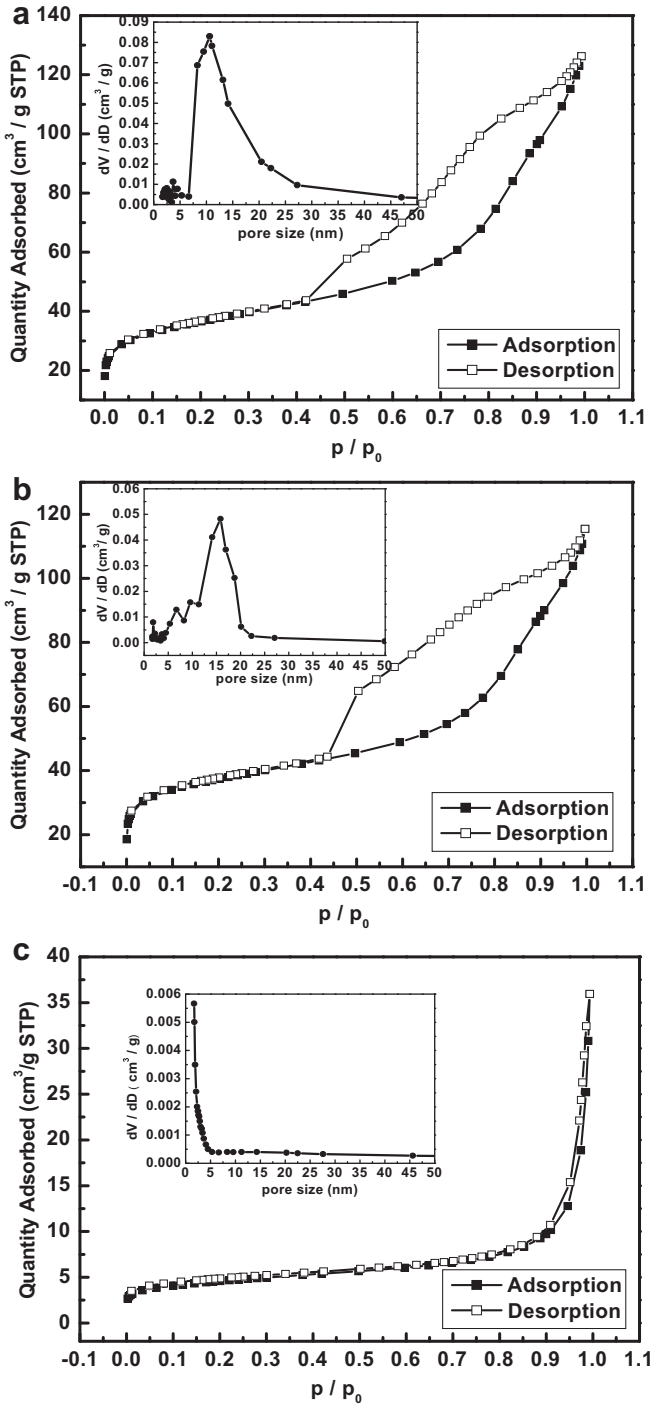

Fig. 3. Nitrogen ad/desorption isotherms of the $LiFePO_4$/C composites; inset: pore size distributions from BJH method; (a) LFP-OC; (b) LFP-DC; (c) LFP-IC.

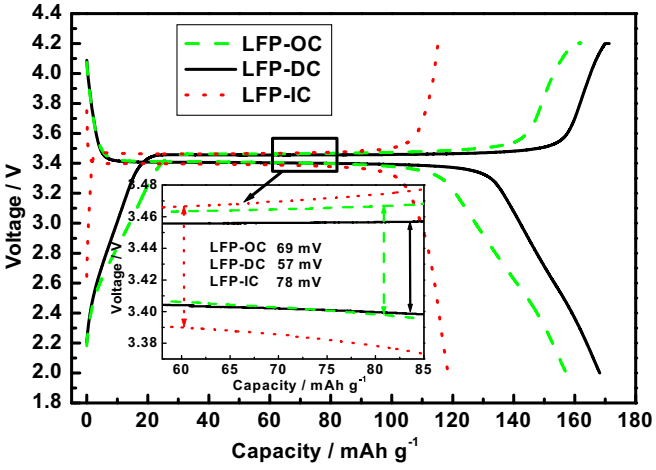

Fig. 4. Initial charge/discharge curves and amplified voltage flats (inset) of the composites at 0.1 C.

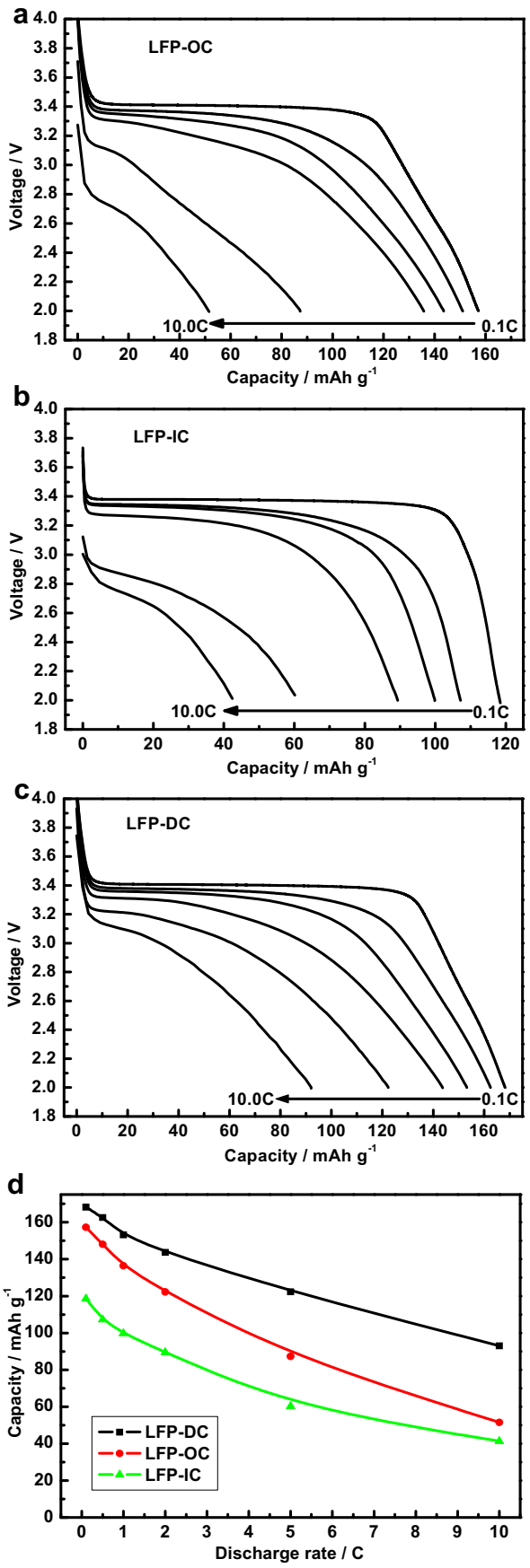

Fig. 5. Initial discharge curves of LFP-OC (a), LFP-IC (b), LFP-DC (c) And their discharge capacities at various discharge rates: 0.1, 0.5, 1.0, 2.0, 5.0 and 10.0 C (d).

Table 2
Discharging capacities of the $LiFePO_4$/C materials reported in 2011.

Capacity (mAh g^{-1})			Synthesis method	Ref.
0.1 C	1 C	5 C		
168	153	122	Our work	
–	140	120	Hydrothermal method	[28]
–	156	124	Hydrothermal method	[29]
167	145	120	Hydrothermal method	[30]
155	–	95	Hydrothermal method	[31]
162	146	121	Solvothermal method	[32]
135	130	–	Polyol-assisted solvothermal method	[33]
147	140	110	Sol–gel method	[34]
162	148	–	Sol–gel method	[35]
137	–	80	Solution method	[36]
160	142	120	Microwave-assisted solution	[37]
149	–	127	Co-precipitation and in-situ polymerization	[38]
155	133	105	High temperature solid state method	[12]
168	150	134	High temperature solid state method – CVD	[39]
150	135	110	Mechanical activation method	[40]

3.5. Electrochemical characterization

Fig. 4 shows initial charge–discharge profiles of the synthesized $LiFePO_4$/C composites in the voltage range of 2.0–4.2 V at a current rate of 0.1 C. It is seen that all the initial charge–discharge curves exhibit a voltage plateau at 3.4–3.5 V, and the specific discharge capacities of LFP-OC, LFP-DC and LFP-IC are 157.2, 168.2 and 118.5 mAh g^{-1}, respectively. The voltage plateau at 3.4–3.5 V confirms that the synthesized composite material is $LiFePO_4$, as discussed in the XRD section. The polarization between charge/discharge plateau at 0.5 Li insertion/extraction of LFP-OC, LFP-DC and LFP-IC is 69, 57 and 78 mV, respectively, indicating that the kinetics is optimal for the $LiFePO_4$/C composite synthesized with the dual carbon sources [13,27]. Coincidently, LFP-DC further yields the highest specific discharge capacity, which is approximate to the theoretical value of $LiFePO_4$. Actually, it is unsurprising that the best electrochemical performance is achieved when the dual carbon sources are used. First, the usage of dual carbon sources yields a molecular mixture of Li^+/e^- conductors in the composite, which lowers charge transfer resistance. Second, the smaller crystallite in the composite further shortens the diffusion length of the Li ions in the electrode. Third, the presence of mesopores and high specific surface area can facilitate the entrance of electrolyte, which improves the interfacial contact between the electrode and the electrolyte.

Fig. 5 shows the discharge profiles at various current rates. To ensure identical initial conditions for each discharging, all the samples were first charged to 4.2 V at 0.1 C rate, and then charged at the constant potential at 4.2 V until the current decreased to 0.05 C. As shown in Fig. 5a,b, the discharge curve of LFP-OC and LFP-IC is seriously bent downward especially at high discharge rates; whereas LFP-DC exhibits a moderate decrease at the same rate. Specifically, no clear voltage plateaus can be recognized in the discharge curves of LFP-OC and LFP-IC at 10 C, for which the discharge capacities are ca. 52 and 42 mAh g^{-1}, respectively. In comparison, LFP-DC shows a remarkable voltage plateau above

Table 3
Carbon content, specific surface area, grain size and electronic conductivity of the three samples prepared with different carbon source contents.

Sample	Residual carbon (wt. %)	Specific surface area (m^2 g^{-1})	Grain size (nm)	Conductivity (S cm^{-1})
LFP-DC-I	14.5	119.7	30.9	6.2×10^{-3}
LFP-DC	14.2	114.9	31.6	2.4×10^{-2}
LFP-DC-II	14.3	51.6	44.8	5.1×10^{-2}

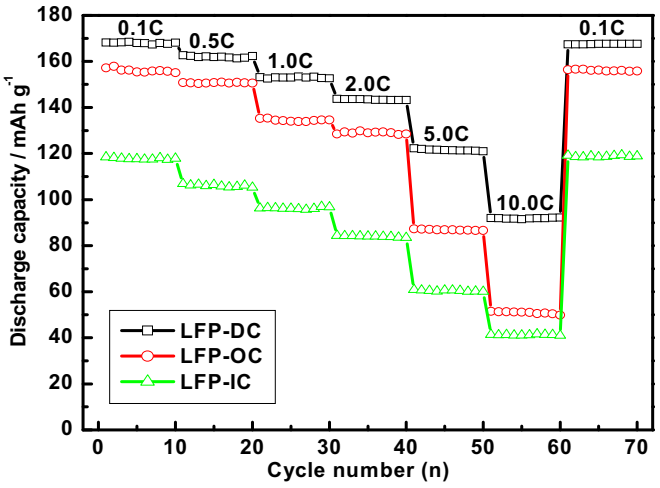

Fig. 6. Discharge capacity retentions of LFP-OC, LFP-DC and LFP-IC at various rates: 0.1, 0.5, 1.0, 2.0, 5.0 and 10.0 C.

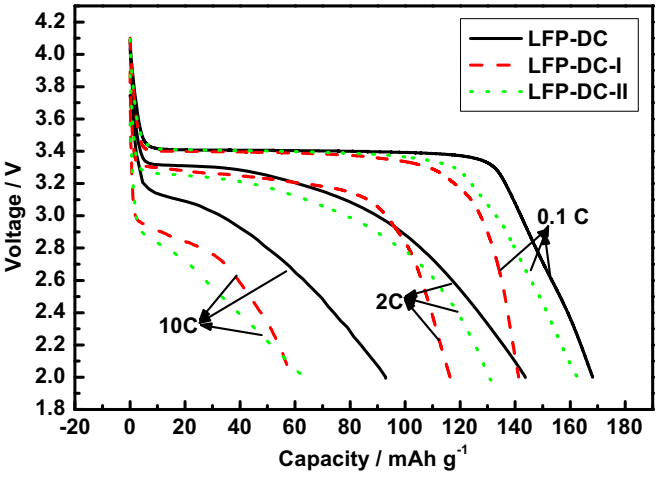

Fig. 7. Initial discharge curves of LFP-DC, LFP-DC-I and LFP-DC-II at various rates: 0.1, 2.0 and 10.0 C.

3.0 V at the same rate, and a high capacity of 93 mAh g^{-1} is also achieved. Fig. 5d clearly reveals that LFP-DC yields superior rate performance to both LFP-OC and LFP-IC. It should be noted that $LiFePO_4$/C synthesized by our method outperforms most samples reported in very recent open literature, as shown in Table 2. As shown in Ref. [28–32,39], high-performance $LiFePO_4$/C composite materials can be synthesized by either the hydrothermal/solvothermal method or the CVD post-treatment. However, it should be noted that these methods are not applicable for the mass production of the $LiFePO_4$/C composite materials, mostly due to the cost issue. The method developed by this work does not include any expensive chemicals or facilities, which is thus a facile, low-cost, and scalable method to synthesize the high-performance $LiFePO_4$/C composite material.

Fig. 6 shows the discharge capacity retentions of the synthesized composites at various rates. It can be seen that all the three composites exhibit rather reproducible capacities during 10-cycle test at each current rate. And the capacity can be retrieved when the lower current rate (0.1 C) is applied again. This result confirms that this synthesis method is reliable to produce stable $LiFePO_4$/C composites. Furthermore, it is clear that the $LiFePO_4$/C composite prepared with dual carbon sources shows superior rate capability to the one prepared with the sole carbon source, especially at high current rates. For example, from 2 to 5 C, the discharge capacities of LFP-OC, LFP-DC and LFP-IC are decreased by 28.5%, 14.8% and 32.6%, respectively. The superior rate capability of LFP-DC can be attributed to both the improved electronic conductivity and the shortened ion diffusion length in the composite [9]

We further studied the effect of the carbon source content on the electrochemical performance while keeping the same total carbon content in the final LFP-DC composite. Fig. 7 presents the discharge curves of the LFP-DC, LFP-DC-I and LFP-DC-II composites. It is seen that the carbon source content yields considerable effect on the electrochemical performance of the composite. For example, the discharge capacity is 168.2, 162.5 and 141.3 mAh g^{-1} for LFP-DC, LFP-DC-I and LFP-DC-II at 0.1 C rate, respectively. By using 50.0 g glucose and 5.0 g XC-72R as the carbon source, the prepared $LiFePO_4$/C composite (viz. LFP-DC) exhibits the best electrochemical performance, especially at higher current rates. The result can be understood based on the properties of the synthesized materials. Table 3 lists the key parameters of the three composites. It is seen that the LFP-DC composite shows a compromise in the specific surface area, grain size and electronic conductivity. Based on the optimization, the sample LFP-DC yields the best electrochemical performance.

3.6. Formation mechanism of LFP-DC

A schematic illustration is provided in Scheme 1 to understand the formation mechanism of the high-performance $LiFePO_4$/C composite with the dual carbon sources. First, the precursor molecules, glucose and XC-72 carbon powders are mixed to form a homogenous solution. Second, the solution is spray-dried, yielding

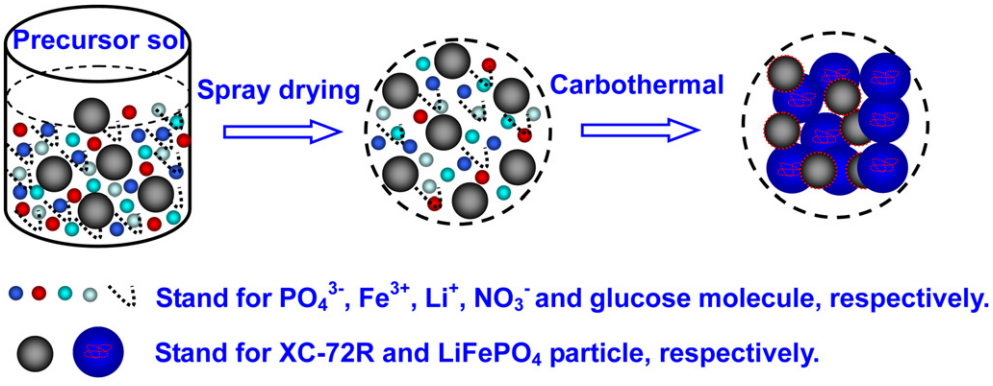

Scheme 1. Formation mechanism of the $LiFePO_4$/C composite material by using the dual organic/inorganic carbon sources.

porous microspherical precursor aggregates. Finally, glucose is carbonized and $LiFePO_4$/C is synthesized.

In the second step, porous microspherical precursor aggregates are formed during the spray drying process, leaving the precursors uniformly mixed at a molecular level. Upon the following pyrolysis, the carbonization of glucose yields the mesopores in the composite materials, and the resultant amorphous carbon is uniformly coated on the $LiFePO_4$ nanocrystallites, which prevents the grains against growing up in size. As a result, the mesoporous $LiFePO_4$/C composite material with a small grain size and high specific surface area is synthesized by this method. On the other hand, the LFP-DC composite material features a high electron conductivity, which can be understood as follows. The spray drying offers a fast solvent evaporation, leaving all precursor species uniformly dispersed in the aggregates. Therefore, it is understandable that the evenly dispersed XC-72R carbon particles facilitate the electron conduction in the aggregates.

4. Conclusions

In this work, the high-performance $LiFePO_4$/C composite material was successfully synthesized in a facile method. We found that the carbon sources yielded a pronounced effect on the morphology, microstructure and the electrochemical performance of the $LiFePO_4$/C composite. Specifically, by using the dual inorganic/organic carbon sources, the synthesized $LiFePO_4$/C composite featured nanometer-sized particles, large specific surface area, mesoporous nature and decent electronic conductivity, which facilitated the ion/electron diffusion in the electrode and thereby yielded the best polarization performance and rate capability in LIBs.

Acknowledgments

The authors thank the National Nature Science Foundation of China (NFSC) (Project Nos. 20876062, 21076089, 21003052) and the Fundamental Research Funds for the Central Universities (SCUT) for financial support. We also thank Dr. Hao Li for the SEM observations, as well as Guangzhou Great Power Co., Ltd. and Guangzhou Tinci Material Technology Co., Ltd. for their help.

Appendix A. Supplementary material

Supplementary data associated with this article can be found, in the online version, at doi:10.1016/j.jpowsour.2012.03.090.

References

[1] A.K. Padhi, K.S. Nanjundaswamy, J.B.J. Goodenough, Electrochem. Soc. 144 (1997) 1188–1194.
[2] A.S. Andersson, J.O. Thomas, B. Kalska, L. Haggstrom, Electrochem. Solid-State Lett. 3 (2000) 66–68.
[3] J.M. Tarascon, M. Armand, Nature 414 (2001) 359–367.
[4] F. Cheng, J. Liang, Z. Tao, J. Chen, Adv. Mater. 23 (2011) 1–21.
[5] S.Y. Chung, J.T. Bloking, Y.M. Chiang, Nat. Mater. 1 (2002) 123–128.
[6] P.P. Prosini, M. Lisi, D. Zane, M. Pasquali, Solid State Ionics 148 (2002) 45–51.
[7] C.M. Doherty, R.A. Caruso, B.M. Smarsly, P. Adelhelm, C.J. Drummond, Chem. Mater. 21 (2009) 5300–5306.
[8] C.M. Doherty, R.A. Caruso, C.J. Drummond, Energy Environ. Sci. 3 (2010) 813–823.
[9] B. Huang, X.D. Zheng, D.M. Jia, M. Lu, Electrochim. Acta 55 (2010) 1227–1231.
[10] N.N. Sinha, C. Shivakumara, N. Munichandraiah, ACS Appl. Mater. Inter. 2 (2010) 2031–2038.
[11] X.L. Wu, L.Y. Jiang, F.F. Cao, Y.G. Guo, L.J. Wan, Adv. Mater. 21 (2009) 2710–2714.
[12] J. Zhao, J. He, J. Zhou, Y. Guo, T. Wang, S. Wu, X. Ding, R. Huang, H.J. Xue, Phys. Chem. C 115 (2011) 2888–2894.
[13] K. Saravanan, M.V. Reddy, P. Balaya, H. Gong, B.V.R. Chowdari, J.J.J. Vittal, Mater. Chem. 19 (2009) 605–610.
[14] Y. Wang, Y. Wang, E. Hosono, K. Wang, H. Zhou, Angew. Chem. Int. Edt. 47 (2008) 7461–7465.
[15] F. Yu, J.J. Zhang, Y.F. Yang, G.Z. Song, J. Power Sources 189 (2009) 794–797.
[16] K. Konstantinov, S. Bewlay, G.X. Wang, M. Lindsay, J.Z. Wang, H.K. Liu, S.X. Dou, J.H. Ahn, Electrochim. Acta 50 (2004) 421–426.
[17] F. Yu, J.J. Zhang, Y.F. Yang, G.Z. Song, J. Mater. Chem. 19 (2009) 9121–9125.
[18] F. Yu, J.J. Zhang, Y.F. Yang, G.Z. Song, Electrochim. Acta 54 (2009) 7389–7395.
[19] F.F. Cao, X.L. Wu, S. Xin, Y.G. Guo, L.J. Wan, J. Phys. Chem. C 114 (2010) 10308–10313.
[20] R. Dominko, M. Bele, M. Gaberscek, M. Remskar, D. Hanzel, J.M. Goupil, S. Pejovnik, J. Jamnik, J. Power Sources 153 (2006) 274–280.
[21] R. Dominko, M. Bele, J.M. Goupil, M. Gaberscek, D. Hanzel, I. Arcon, J. Jamnik, Chem. Mater. 19 (2007) 2960–2969.
[22] Y.S. Hu, Y.G. Guo, R. Dominko, M. Gaberscek, J. Jamnik, J. Maier, Adv. Mater. 19 (2007) 1963–1966.
[23] D. Choi, P.N. Kumta, J. Power Sources 163 (2007) 1064–1069.
[24] M.M. Doeff, J.D. Wilcox, R. Yu, A. Aumentado, M. Marcinek, R. Kostecki, J. Solid State Electrochem. 12 (2008) 995–1001.
[25] J.D. Wilcox, M.M. Doeff, M. Marcinek, R. Kostecki, J. Electrochem. Soc. 154 (2007) A389–A395.
[26] L.Q. Sun, M.J. Li, R.H. Cui, H.M. Xie, R.S. Wang, J. Phys. Chem. C 114 (2010) 3297–3303.
[27] F. Yu, J. Zhang, Y. Yang, G. Song, J. Power Sources 195 (2010) 6873–6878.
[28] M. Wang, Y. Yang, Y. Zhang, Nanoscale 3 (2011) 4434–4439.
[29] H. Shu, X. Wang, Q. Wu, B. Ju, L. Liu, X. Yang, Y. Wang, Y. Bai, S. Yang, J. Electrochem. Soc. 158 (2011) A1448–A1454.
[30] F. Lu, Y.C. Zhou, J. Liu, Y. Pan, Electrochim. Acta 56 (2011) 8833–8838.
[31] C. Su, L. Xu, B. Wu, C. Zhang, Electrochim. Acta 56 (2011) 10204–10209.
[32] Q. Wang, W. Zhang, Z. Yang, S. Weng, Z. Jin, J. Power Sources 196 (2011) 10176–10182.
[33] J. Lim, D. Kim, V. Mathew, D. Ahn, J. Kang, S.W. Kang, J. Kim, J. Alloys Compd. 509 (2011) 8130–8135.
[34] F.F. Pan, W.L. Wang, H.J. Li, X.D. Xin, Q.Q. Chang, W.S. Yan, D. Chen, Electrochim. Acta 56 (2011) 6940–6944.
[35] H.Y. Gao, L.F. Jiao, W.X. Peng, G. Liu, J.Q. Yang, Q.Q. Zhao, Z. Qi, Y.C. Si, Y.J. Wang, H.T. Yuan, Electrochim. Acta 56 (2011) 9961–9967.
[36] G. Hasegawa, Y. Ishihara, K. Kanamori, K. Miyazaki, Y. Yamada, K. Nakanishi, T. Abe, Chem. Mater. 23 (2011) 5208–5216.
[37] I. Bilecka, A. Hintennach, M.D. Rossell, D. Xie, P. Novak, M. Niederberger, J. Mater. Chem. 21 (2011) 5881–5890.
[38] W. Ying, B. Sun, J. Park, W.S. Kim, H.S. Kim, G.X. Wang, J. Alloys Compd. 509 (2011) 1040–1044.
[39] C.Y. Wu, G.S. Cao, H.M. Yu, J. Xie, X.B. Zhao, J. Phys. Chem. C 115 (2011) 23090–23095.
[40] Y. Yin, M. Gao, H. Pan, L. Shen, X. Ye, Y. Liu, P.S. Fedkiw, X. Zhang, J. Power Sources 199 (2012) 256–262.